

1 **Longitudinal and seasonal variations in plasmaspheric electron density:**
2 **Implications for electron precipitation.**

3
4 M. A. Clilverd, N. P. Meredith, R. B. Horne, S. A. Glauert

5 British Antarctic Survey,

6 Natural Environment Research Council,

7 Madingley Road, Cambridge, CB3 0ET, England.

8 macl@bas.ac.uk, nmer@bas.ac.uk, rh@bas.ac.uk, sagl@bas.ac.uk

9
10 R. R. Anderson,

11 Department of Physics and Astronomy,

12 The University of Iowa, Iowa City, Iowa, IA 52242-1479.

13 roger-r-anderson@uiowa.edu

14
15 N.R. Thomson

16 Department of Physics,

17 University of Otago,

18 Dunedin, New Zealand.

19 n_thomson@physics.otago.ac.nz

20
21
22 F. W. Menk,

23 Department of Physics,

24 University of Newcastle,

25 Newcastle, NSW

26 Australia

27 Fred.Menk@newcastle.edu.au

28
29 B. R. Sandel,

30 Lunar and Planetary Laboratory,

31 The University of Arizona,

32 Sonett Space Sciences Building,

33 1541 East University Boulevard,

34 Tucson,

35 AZ 85711-0063, U.S.A.

36 sandel@arizona.edu

37
38 Abstract: The tilt and offset of the Earth's magnetic field can significantly affect the

39 longitudinal and seasonal distribution of electron density in the plasmasphere. Here

40 we show that for the solar maximum conditions of 1990-91, the largest annual

41 variation determined from CRRES measurements of plasmaspheric equatorial

42 electron density in the range $L=2.5-5.0$ occurs at American longitudes (-60°E), while

43 no annual variation occurs at Asian longitudes ($+100^\circ\text{E}$). Plasmaspheric electron

44 density is larger in December than in June at most longitudes, from -180°E eastwards

45 to +20°E. At all other longitudes the density ratio from December to June is very
46 close to 1.0. The largest December/June density ratio is at L=3.0 at American
47 longitudes (-60°E). At L=4.5 and above, the annual variation disappears. The lowest
48 electron density values for a given L-shell occur at American longitudes, in June. Ion
49 densities also show significant annual variations, with similar longitudinal and
50 seasonal characteristics in the case of IMAGE EUV He⁺ measurements. Atomic mass
51 density measurements calculated using the magnetometer cross-phase technique show
52 significant seasonal variations, but also imply composition changes with longitude.
53 Using the quasilinear PADIE code we calculate the bounce-averaged diffusion rate of
54 electrons by plasmaspheric hiss with a fixed wave intensity. December to June
55 variations in plasmaspheric density, particularly at American longitudes, drive
56 changes in the wave-particle interactions, increasing diffusion into the loss cone by a
57 factor of ~3 at 1 MeV at L=3.0, thus hardening the electron precipitation spectrum
58 during the southern hemisphere winter (in June).
59

59 Introduction

60

61 The plasmasphere is a region of low energy ('cold' i.e., $T_e \sim 1$ eV) plasma
62 surrounding the Earth, and extending out to $L \sim 2-6$ depending on geomagnetic
63 latitude, geomagnetic disturbance levels, and on local time. It is primarily made up of
64 electrons and protons that have diffusively migrated from the underlying ionosphere.
65 Overlapping the plasmasphere are regions of high energy ('hot' i.e., $T_e \sim 1$ MeV)
66 plasma known as the radiation belts. Low frequency radio waves propagating within
67 the plasmasphere can interact with the high energy radiation belt particles, changing
68 their energy spectra and causing them to precipitate into the Earth's upper
69 atmosphere, driving chemical changes [e.g., Rosanov et al., 2005]. Variability in the
70 background conditions of the plasmasphere is one of the factors in determining the
71 efficiency of wave-particle interactions [e.g., Horne et al., 2003], thus influencing the
72 resultant particle precipitation into the atmosphere. Here we use CRRES satellite
73 measurements of 'cold' plasmaspheric equatorial electron density to investigate the
74 longitudinal and annual variations in density in the range $L=2.5-5.0$, and assess the
75 effect on the rate of 'hot' electron precipitation from the overlapping outer radiation
76 belt.

77

78 The annual variation in equatorial plasmaspheric electron density (N_{eq}) has been
79 observed previously. The first observations were made using natural whistler signals,
80 typically at either American or European longitudes [e.g., Helliwell, 1965; Park et al.,
81 1978; Tarcsai et al., 1988]. In these cases N_{eq} showed a maximum in December and a
82 minimum in June, with December larger by a factor of between 1.5-3.0 at $L=1.5-2.5$,
83 depending on longitude.

84

85 Man-made whistler-mode signals from US Naval transmitters were analysed by
86 Clilverd et al. [1991] and showed a December to June ratio of Neq of 3.0 (2.0) at solar
87 minimum (maximum) at L=2.5 in the American longitude sector, and a ratio of 1.4 at
88 solar maximum in the New Zealand/Pacific longitude sector. Using conjugate
89 ionosonde pairs such as Wallops Island (37.9°N, 75.5°W, L=2.39) and Argentine
90 Islands (65.3°S, 64.3°W, L=2.44) Clilverd et al. [1991] showed that the seasonal Neq
91 variation was largest at 300°E geographic (-60°E) because at that longitude the offset
92 of the geomagnetic field configuration relative to geographic coordinates is largest.
93 Calculations showed that each field line flux tube is in long-term diffusive
94 equilibrium with the underlying ionospheres at the footprints of the field line and the
95 annual behaviour of the plasmasphere reflects the local annual variation of the
96 northern and southern F2 regions linked to it. In Figure 1 we show this variation of the
97 geographic latitude of the footprints of the L=2.5 field line contour, using the IGRF
98 magnetic field model, as a function of geographic longitude. The southern L=2.5
99 contour at -60°E has an underlying ionosphere that is at high latitude and thus
100 continually sunlit during the December solstice, and in near continuous darkness
101 during the June solstice. These factors, along with differing horizontal thermospheric
102 winds at such high geographic latitudes driving the ionospheric plasma up the field
103 lines, produce significant changes in plasmaspheric density from solstice to solstice.
104 Clilverd et al. [1991] also suggested that there would be no annual variation at
105 African/Asian longitudes, and that in June global Neq values at L=2.5 would be
106 largely independent of longitude and similar to that observed at -60°E, i.e., ~1000
107 el.cm⁻³.

108

109 The annual variation in Neq has been modelled with a view to reproducing the
110 observations, and understanding the underlying physical processes responsible. Some
111 models reproduced the December/June annual variation at American longitudes, and
112 then made predictions regarding the effect at other longitudes. Early work by
113 Rasmussen and Schunk [1990] showed a Neq maximum in June rather than December
114 as is actually observed – probably because of the centred dipole model used.
115 Modelling work undertaken by Rippeth et al. [1991], which included a tilted offset
116 dipole in the model, was better able to reproduce the observations at L=2.5 at
117 American longitudes. Guiter et al. [1995] modelled plasmaspheric densities at L=2
118 and found that Neq was 1.5 times higher in December than in June for 300°E (-60°E)
119 longitude. At 120°E longitude the L=2 Neq was predicted to be higher in June than
120 December by a factor of 1.2. The underlying mechanism driving the annual variation
121 was considered to be variations in ionospheric O⁺.

122

123 Further modelling using the field line interhemispheric model (FLIP) indicated that
124 the annual variation at American and Australian longitude sectors were likely to be 6
125 months out of phase [Richards et al., 2000]. This work concluded that plasmaspheric
126 thermal structure, not ionospheric density, should play a key role in producing the
127 annual variation at solar minimum. A new approach using dynamical diffusive
128 equilibrium, called the global plasmasphere ionosphere density model (GPID), was
129 able to reproduce the observed seasonal variations in Neq at L=2.5 during solar
130 maximum, but not at solar minimum [Webb and Essex, 2001].

131

132 To maintain charge neutrality an annual variation in ion concentration would be
133 anticipated. Berube et al. [2003] used data from a pair of magnetometers at L=1.74 in

134 the MEASURE array (American longitudes) to determine the plasmaspheric
135 equatorial mass density. They observed an annual variation in mass density with
136 December densities 2-3 times higher than in June. This suggests that the mass
137 densities vary in a similar way to the electron densities. Although at $L < 2$, the annual
138 variation in field line resonance frequencies is due to the influence of O^+ in the
139 underlying ionosphere changing the Alfvén speed profile along those flux tubes
140 [Waters et al., 1994].

141

142 Here we perform a comprehensive study of the longitudinal and seasonal variation
143 of the equatorial plasmaspheric electron density in the region $2.5 < L < 5.0$ using data
144 from the CRRES satellite. We examine the observed N_{eq} radial profiles during solar
145 maximum conditions (1990/91) at different longitudes and at different times of year,
146 and compare the profiles against the commonly used profiles of Carpenter and
147 Anderson, 1992. We also investigate the equivalent mass density variations using the
148 IMAGE EUV measurements of He^+ , and atomic mass from the cross-phase analysis
149 of ground-based magnetometer data. The relevance of the plasmaspheric density
150 variations are put into the context of changing wave-particle interactions, and the
151 subsequent deposition of energetic particles into the upper atmosphere.

152

153

153

154

155 Determination of electron densities in the plasmasphere

156

157 Electron number densities are derived from wave data provided by the Plasma Wave

158 Experiment on board the Combined Release and Radiation Effects Satellite (CRRES).

159 This satellite, which was launched on 25 July 1990, operated in a highly elliptical

160 geosynchronous transfer orbit with a perigee of 305 km, an apogee of 35,768 km and

161 an inclination of 18°. The orbital period was approximately 10 hours, and the initial

162 apogee was at a magnetic local time (MLT) of 0800 MLT. The magnetic local time of

163 apogee decreased at a rate of approximately 1.3 hours per month until the satellite

164 failed on 11 October 1991, when its apogee was at about 1400 MLT. The satellite

165 swept through the plasmasphere on average approximately 5 times per day for almost

166 15 months. The Plasma Wave Experiment provided measurements of electric fields

167 from 5.6 Hz to 400 kHz, using a 100 m tip-to-tip long wire antenna, with a dynamic

168 range covering a factor of at least 10^5 in amplitude [Anderson et al., 1992].

169

170 The sweep frequency receiver, which is used in this study, covered the frequency

171 range from 100 Hz to 400 kHz in four bands with 32 logarithmically spaced steps per

172 band, the fractional step separation being about 6.7% across the entire frequency

173 range. Band 1 (100 Hz to 810 Hz) was sampled at one step per second with a

174 complete cycle time of 32.768 s. Band 2 (810 Hz to 6.4 kHz) was sampled at two

175 steps per second with a complete cycle time of 16.384 s. Band 3 (6.4 to 51.7 kHz) and

176 band 4 (51.7 kHz to 400 kHz) were sampled 4 times per second with complete cycling

177 times of 8.192 s.

178 The electron number density is determined from the electron plasma frequency, f_{pe} ,
179 using the standard expression $n_e = 4\pi^2 f_{pe}^2 \epsilon_0 m_e / e^2$. When emissions at the upper hybrid
180 frequency, f_{uhr} , are well-defined the electron plasma frequency, f_{pe} , is derived from f_{uhr}
181 using the relationship $f_{pe}^2 = f_{uhr}^2 - f_{ce}^2$, where f_{ce} is the electron gyrofrequency,
182 determined from the CRRES fluxgate magnetometer [Singer et al., 1992]. When the
183 upper hybrid frequency cannot be identified the electron plasma frequency is
184 estimated from the lower frequency limit of the electromagnetic continuum radiation,
185 which is taken to be the plasma wave cutoff at the plasma frequency [Gurnett and
186 Shaw, 1973]. The number densities are initially determined at a temporal resolution of
187 8.192 s and subsequently averaged as a function of half orbit (inbound or outbound)
188 and L in steps of 0.1L. The position of the CRRES spacecraft is mapped to the
189 ionosphere at the same temporal resolution using the IGRF 85 model corrected for
190 external magnetospheric currents by the Olson-Pfizer tilt dependent static model
191 [Olson and Pfizer, 1977]. This is the standard process used to analyze all CRRES
192 data. The geographic coordinates are then averaged as a function of half orbit and L
193 shell in steps of 0.1L. The time in UT, magnetic latitude, magnetic local time and time
194 spent in each bin are also recorded at the same resolution.

195

196 The resulting database is subsequently analysed to determine the behaviour of the
197 plasmaspheric equatorial number density as a function of geographic longitude and
198 for different L shells and seasons. Throughout this paper we use geographic longitude
199 during discussions of the results and the figures shown. We focus on periods centred
200 near the solstices and use the data from October to February (inclusive) for the
201 December solstice and from April to August (inclusive) for the June solstice. For each
202 season the data are averaged into bins that are 5° in geographic longitude for L shells

203 ranging from 2.5 +/- 0.3 L to 5.0 +/- 0.3 L in steps of 0.5L. The data are included in
204 the averaging process only when the measurements are made within the plasmasphere
205 and when the magnetic latitude of the CRRES spacecraft lies within +/- 10° of the
206 magnetic equator.

207

208 Data are selected to be in the plasmasphere using a criterion based on the amplitude
209 of the waves in the frequency band $f_{ce} < f < 2f_{ce}$. Waves in this frequency band, which
210 contains contributions from both electron cyclotron harmonic waves and thermal
211 noise, tend to be excluded from the high density region inside the plasmopause.
212 Specifically observations in the plasmasphere are identified using the criterion that the
213 wave amplitude for frequencies in the range $f_{ce} < f < 2f_{ce}$ must be less than 0.0005
214 mV m^{-1} [Meredith et al., 2004]. Observations made in regions where this criterion did
215 not hold are assumed to be outside the plasmopause at the time and are excluded from
216 the analysis. In practice although we exclude data during large geomagnetic storms
217 using the wave amplitude criterion we will include some density values when the
218 plasmasphere is likely to be in an intermediate refilling state following the storms.
219 Overall, our criterion for selecting plasmaspheric measurements is somewhat
220 conservative in that we reject ~14% of the data where the ECH waves in the range f_{ce}
221 $< f < 2f_{ce}$ have amplitudes above 0.0005 mV m^{-1} but the densities are likely to be
222 representative of the plasmasphere at the time [Meredith et al., 2004]. However, this
223 criterion does reduce the number of low density measurements included in our
224 analysis where the plasmopause is ill-defined, and when the plasmasphere is subject to
225 erosion during geomagnetically active periods (i.e., $AE > 100$ nT).

226

227 Determination of ion densities in the plasmasphere

228

229 The ion mass densities presented in this study were calculated using field-line
230 resonant frequencies (FLRs) measured from pairs of ground-based magnetometers,
231 following the analytical expressions described by Taylor and Walker [1984] and
232 Walker et al. [1992]. These assume decoupled toroidal mode oscillations and yield
233 essentially identical results to the models described by Orr and Matthew[1971].
234 Techniques for the detection of FLRs were summarized by Menk et al. [1999] and
235 Menk et al. [2000]. When examining data from latitudinally-separated
236 magnetometers, the resonant frequency is identified by the peak in H-component
237 cross-power and cross-phase, and a unity crossing in H-component power ratio,
238 approximately mid-way between the stations. Where only one station is available the
239 resonance is indicated by a peak in the power ratio H/D and a rapid change in
240 polarization i.e., in the phase between the H and D components.

241

242 The uncertainty in our calculated mass densities presented in this study (20-
243 30%) depends mainly on uncertainty in the frequency measurement with uncertainties
244 typically of order 10-15%. Menk et al. [1999] discussed the relationship between
245 these two uncertainties and found the mass density uncertainty to be typically double
246 the uncertainty in frequency measurement. We have assumed a dipole magnetic field,
247 and at L=2.5 this introduces negligible error.

248

249 Measurements of the He⁺ ion density presented in this study were made with
250 the Extreme Ultraviolet Imager (EUV Imager) on-board the IMAGE spacecraft, by
251 detecting its resonantly-scattered emission at 30.4 nm [Sandel et al., 2001]. The
252 IMAGE spacecraft is in an elliptical polar orbit with an apogee altitude of 7.2 Earth

253 radii (46,000 km) and a perigee altitude of 1,000 km, and completes one orbit every
254 14.2 hours. Effective imaging of the plasmaspheric He⁺ requires global 'snapshots' in
255 which the high apogee and the wide field of view of the EUV Imager provide in a
256 single exposure a map of the entire plasmasphere. The 30.4 nm feature is relatively
257 easy to measure because it is the brightest ion emission from the plasmasphere, it is
258 spectrally isolated, and the background at that wavelength is negligible. Line-of-sight
259 measurements are easy to interpret because the plasmaspheric He⁺ emission is
260 optically thin, so its brightness is directly proportional to the He⁺ column abundance.
261 The EUV Imager instrument consists of three identical sensor heads, each having a
262 field of view of 30°. These sensors are tilted relative to one another to cover a fan-
263 shaped field of 84° x 30° that is swept across the plasmasphere by the spin of the
264 satellite. EUV Imager's spatial resolution is ~0.6° or ~0.1 Re in the equatorial plane
265 seen from apogee. The sensitivity is sufficient to map the position of the plasmopause
266 with a time resolution of 10 minutes or better.

267

268 For this study we selected EUV measurements from times in June and
269 December 2001. We used 122 images taken from the period 15-17 June and 97
270 images from the period 9-20 December. All images were from quiet times ($K_p \leq 2$),
271 chosen to avoid azimuthal structures that often appear during more active times. After
272 transforming each image to the plane of the magnetic equator [Sandel et al., 2003]
273 using magnetic longitude as the azimuthal coordinate, we summed the images to a
274 single image for each of June and December. The summation omitted the region of
275 Earth's shadow and the overlaps between the three EUV cameras.

276

277 We derived azimuthal profiles of brightness vs. magnetic longitude by
278 sampling these composite images in an annulus of width $0.3 L$ centered at $L=2.5$ with
279 a bin size of 5° in magnetic longitude. To infer equatorial He^+ abundances from the
280 measured brightness, we used the concept of effective path length described by
281 Clilverd et al. [2003] and Gallagher et al. [2005].

282

283 Longitudinal and seasonal variations in plasmaspheric densities

284

285 Figure 2 shows the density variation with longitude from CRRES for December
286 (solid line) and June (dashed line) for $L=2.5-5.0$. Some of the data shown for
287 December at $L=2.5$ are indicated by a dot-dashed line, indicating that they are less
288 reliable than the other data. The densities at these longitudes in December were so
289 large ($>2000 \text{ el. cm}^{-3}$) that the upper hybrid frequency could not be determined at all
290 times, and data from a higher range of L-shells ($L=2.7-3.3$) were used and linearly
291 extrapolated to $L=2.5$ and shown as the dot-dashed line. Thus the data should be
292 treated as less reliable than the rest shown. However, the same extrapolation
293 technique used on the $L=2.5$ June data, and some of the other panels ($L=3.0-4.0$)
294 reproduced the December data to within 5%. We make this extrapolation for the
295 $L=2.5$ December data primarily to allow comparison with previous work, it does not
296 materially affect any of the conclusions from this paper.

297

298 For $L=2.5-3.5$ it is clear that the density is much higher in December than June over
299 the longitude range -180°E to 20°E . At the remaining longitudes the December and
300 June densities are much more nearly equal, with occasionally the June densities
301 exceeding the December ones by up to 10%. The same relationship occurs for the

302 higher L-shell regions ($L \sim 4.0$), although the data are more sparse because of
303 incursions by the plasmopause and hence the plots are somewhat less clear. As
304 expected the average density level decreases with increasing L-shell as the plasma
305 from the underlying ionosphere diffuses up into ever increasing flux tube volumes.
306 This is true for each season, and every longitude.

307

308 The largest difference in density between December and June occurs at about -60°E
309 longitude, which is consistent with the conclusions of Clilverd et al. [1991]. At $L=2.5$
310 the densities in June at this longitude are $\sim 1000 \text{ el.cm}^{-3}$, while the December densities
311 are $\sim 2500 \text{ el.cm}^{-3}$. This compares well with the whistler-mode results shown in
312 Clilverd et al. [1991] which were 1400 el.cm^{-3} and $\sim 2800 \text{ el.cm}^{-3}$ respectively in June
313 and December, at solar maximum. The 10-40% systematically higher results from the
314 whistler-mode signals may be due to a slightly lower average L-shell than $L=2.5$, i.e.,
315 $L=2.45$ [Saxton and Smith, 1989]. If the average whistler-mode L-shell used in
316 Clilverd et al. [1991] is 0.05 L equatorward of $L=2.5$ this would make only an 8%
317 difference to the electron density calculations. The extrapolation error of 5% should
318 also be included in this interpretation, suggesting that $\sim 10\%$ of the difference between
319 the two techniques could be due to errors in assumptions made. The remainder may be
320 due to the requirement for whistler-mode signals to propagate in field-aligned electron
321 density enhancements and suggest that duct enhancements maybe typically 20% of
322 the average electron density levels, in agreement with previous ray-tracing
323 calculations of 10-20% [Strangeways, 1991].

324

325 The change in the annual variation of N_{eq} with L-shell is shown in Figure 3 as a
326 ratio of December to June N_{eq} values. Three longitudes are shown, $+100^\circ$ (Asia), -60°

327 (America), and -150°(New Zealand). While not actually at the exact longitude of New
328 Zealand, the longitude (-150°) is used because it is the appropriate longitude for the
329 ‘New Zealand’ ground-based whistler-mode data [Clilverd et al., 1992] which showed
330 an annual variation ratio of ~1.4. At Asian longitudes there is virtually no annual
331 variation, with the Neq ratio staying within ±10% of unity. The American longitudes
332 show a maximum ratio of 2.7 at L=2.5—3.5. By L=4.5 the annual variation in Neq
333 has almost disappeared. The New Zealand longitudes show a relatively small annual
334 variation, with a ratio of about 1.5, with a gradual decline in the effect with increasing
335 L-shell.

336

337 The radial density profile in the plasmasphere is typically represented as an L^{-4}
338 distribution. The following expression based on the plasmaspheric model of Chappell
339 et al. [1970] is used to represent the results obtained from whistler-mode signals:

340

$$341 \quad N_{eq} = 3877 P_e^2 [2/L]^N \quad \text{el.cm}^{-3} \quad (1)$$

342

343 where P_e is a plasma enhancement factor, usually taken as 1.0, N is the radial power
344 law, usually assumed to be 4.0, and 3877 el.cm^{-3} is the electron density at $L=2.0$. The
345 results of least squares fitting of equation (1) to the data for both +100°E (Asia) and -
346 60°E (American) longitudes in December and June is shown in Figure 4. The values
347 of P_e and N are shown in each panel, with the best fit represented by a solid line. The
348 Neq data points are shown by diamonds. A dotted reference line using the empirical
349 Carpenter and Anderson plasmasphere model [Carpenter and Anderson, 1992] for
350 December and June during solar maximum conditions (sunspot number, $R=150$) is
351 also shown. The Carpenter and Anderson model was developed from satellite profiles

352 of N_{eq} that included coverage at $L \leq 3$, and restricted to those profiles where $N_{eq} > 667$
353 el.cm^{-3} at $L = 3$. Profiles were then used until they became irregular at higher L-shells
354 or exhibited a steeper negative slope. This, and the requirement that geomagnetic
355 activity had been low for ~ 20 hours prior to the profile measurement, ensured that the
356 model represents the quiet-time, saturated plasmasphere. But the CRRES results
357 shown in Figure 2 suggest that these electron density restriction at $L = 3$ would reject
358 some saturated plasmasphere conditions found at American longitudes around the
359 time of the June solstice. We would expect our ECH limitation on the CRRES data
360 selection to ensure saturated plasmasphere measurements, but potentially only at L-
361 shells which are typically unaffected by weak or moderate geomagnetic activity ($L <$
362 4).

363

364 In Figure 4 the CRRES data for Asian longitudes ($+100^\circ\text{E}$) show little variation
365 with season, with P_e and N values very close to the normal values used, i.e., 1.0 and 4
366 respectively. At American longitudes (-60°E) there are significant changes in the
367 radial profile from December to June. In December the best fit is given by $P_e=1.6$ and
368 $N=5$. So the $L \leq 3$ density levels are elevated compared with normal values and the
369 radial profile is steeper than expected. In June $P_e=0.75$, and $N=3.4$ and the densities
370 are lower than normal, and the radial profile is less steep. Averaged over longitude at
371 any given time of year the density profiles should look similar to those given by
372 Carpenter and Anderson, because their analysis did not take longitudinal variability
373 into account. In practice this is true for our data until $L > 3.5$, after which the
374 consistently lower densities seen in our data shows clear evidence that our analysis
375 includes some non-saturated density levels, that would have been excluded from the
376 Carpenter and Anderson model.

377

378 The annual variation in electron density should be mirrored in the ion density in
379 order to conserve charge neutrality in the plasmasphere. In Figure 5 we plot the
380 longitudinal and seasonal variation of He^+ abundance derived from the IMAGE EUV
381 experiment [Sandel et al., 2001]. The EUV units are He^+ (cm^{-3}), and are taken from
382 measurements made in June and December 2001. The December EUV values are
383 represented by crosses, with June values by diamonds. The longitudinal variations in
384 He^+ closely match the electron density variations despite being taken from different
385 solar cycles.

386

387 To avoid a bias introduced by the diurnal variation in ion abundance, we
388 aimed to select times for which the phase of the magnetic longitude system was
389 uniformly distributed in magnetic local time. The final set of images chosen was
390 imperfect in this regard. Therefore we assessed the possibility that some of the
391 structure in the EUV measurements in Figure 5 could arise from incomplete averaging
392 of the diurnal variation over all magnetic longitudes. We created a simple model to
393 compute the residual modulation in magnetic longitude that might result from our
394 specific sampling of the diurnal variation. It showed a modulation of lower amplitude,
395 having a shape different from the structure in Figure 5. We conclude that imperfect
396 averaging of the diurnal variation does not significantly bias the structure measured in
397 longitude.

398

399 Ion number densities have been calculated for Figure 5 using cross-phase analysis
400 [Menk et al., 1999] for the longitudes of -65°E and -10°E at $L=2.5$ for December/June
401 2001. These data are shown in Figure 5 as squares (December) and triangles (June),

402 and also indicate a strong annual variation in density at the longitudes observed. The
403 pair of magnetometer stations used for the -65°E values is Millstone Hill and APL
404 from the MEASURE array, and the -10°E values are Hartland and York from the
405 SAMNET array. Both midpoints are close to $L=2.5$, but have been normalised to
406 exactly $L=2.5$ assuming a radial L^{-4} variation. The ion values plotted at -65°E have
407 been adjusted by a factor of 1.3 in order to convert atomic mass units to number
408 densities, and to make the plotted points match the electron densities at that longitude.
409 The adjustment value suggests 11% composition of He^+ and the EUV data suggest
410 $\sim 20\%$. These results are consistent with the H^+/He^+ composition during quiet times.
411 Environmental differences due to different sampling times, and differences due to
412 different techniques may be adequate to account for the differences observed here.
413 However, the ion values at -10°E have been adjusted by a factor of 2.1. Although the
414 data clearly shows the annual variation in density, the adjustment factor is much
415 larger than expected and is consistent with significant heavy ion loading at these
416 longitudes, i.e., about 6% O^+ . However, this result is not inconsistent with the results
417 from Sutcliffe et al. [1987] who found increasing plasma mass density with longitude
418 eastwards towards 20°E in June at $L\sim 1.78$, due to increased O^+ concentrations at 1000
419 km, probably driven by vertical ion drifts from meridional winds in the upper
420 ionosphere.

421

422 Implications for electron precipitation

423

424 The background electron density in the plasmasphere plays a key role in
425 determining the resonant energy of wave-particle interactions. In this section we
426 investigate the influence that the annual variation in electron density will have on

427 pitch-angle scattering of energetic electrons into the loss cone, out of the radiation
428 belts, and subsequent precipitation into the atmosphere.

429

430 Meredith et al. [2006] calculated loss timescales for pitch angle scattering by
431 plasmaspheric hiss using the PADIE code [Glauert and Horne, 2005] with wave
432 properties based on CRRES observations. The determination of the diffusion
433 coefficients requires knowledge of the distribution of the wave power spectral density
434 with frequency and wave normal angle, together with the ratio f_p/f_{ce} , wave mode, and
435 the number of resonances. The ratio f_{pe}/f_{ce} is dependent on the background electron
436 density, and the background magnetic field.

437

438 Here we analyse the effect of differing levels of plasmaspheric density at $L=3.0$ using
439 the PADIE code. Following the analysis of Meredith et al. [2006] we use similar
440 parameters to model the wave interactions. Since energetic outer zone electron loss
441 timescales inside the plasmasphere can be explained by wave particle interactions
442 with plasmaspheric hiss propagating at small or intermediate wave normal angles (ψ),
443 we assume a Gaussian angular spread in X , where $X = \tan \psi$, with a width
444 corresponding to $\psi = 20^\circ$. Since wave propagation at an angle to B is included, we
445 calculate the diffusion rates for Landau ($n=0$) and ± 10 cyclotron harmonic resonances.
446 We assume a wave power of 900 pT^2 and that the wave spectra intensity peaks at 0.55
447 kHz, with a bandwidth of 0.3 kHz and lower and upper cut-offs of 0.1 kHz and 2.0
448 kHz respectively. Following Lyons et al. [1972] we calculate the bounce-averaged
449 diffusion rate which takes into account the scattering of particles in pitch angle over
450 the complete range of latitudes between the mirror points.

451

452 We use values of the ratio f_{pe}/f_{ce} that are equivalent to electron density levels of
453 1500 el.cm^{-3} ($f_{pe}/f_{ce}=10.8$), 1000 el.cm^{-3} ($f_{pe}/f_{ce}=8.8$), and 500 el.cm^{-3} ($f_{pe}/f_{ce}=6.2$).
454 The PADIE code assumes a dipole magnetic field, and we use values of f_{pe}/f_{ce} that
455 are calculated at the $L=3.0$ geomagnetic equator. These density levels represent
456 conditions at $L=3.0$ for American longitudes in December (1500 el.cm^{-3}) and June
457 (500 el.cm^{-3}) taken from Figure 2, and the Asian longitudes for most times of the year
458 (1000 el.cm^{-3}). The pitch angle diffusion coefficients are shown in Figure 6. The
459 f_{pe}/f_{ce} conditions are shown, with the bounce-averaged diffusion coefficient ($\langle D_{\alpha\alpha} \rangle$)
460 plotted against electron pitch angle for 3 different electron energies. At times the
461 bounce-averaged diffusion coefficient becomes extremely small and lies off the plot
462 for large ranges of pitch angle. The 100 keV results for pitch angles $<65^\circ$ (long
463 dashed line) during low plasmaspheric density conditions ($f_{pe}/f_{ce}=6.2$) is an example.
464 The plot shows that for 100 keV electrons the diffusion rate at the edge of the loss
465 cone (vertical dot-dashed line at pitch angles of $\sim 10^\circ$) is reduced by a factor of ~ 5 as
466 the plasmasphere becomes depleted to density levels equivalent of American
467 longitudes around the June solstice. However, 1 MeV electron diffusion rates increase
468 by a factor of ~ 3 . Thus between December and June hiss driven precipitation into the
469 atmosphere will become spectrally harder at American longitudes. At Asian
470 longitudes, represented by $f_{pe}/f_{ce}=8.8$, there would be little change in the
471 precipitation particle energy spectra with season since f_{pe}/f_{ce} hardly changes.

472

473 Discussion

474

475 Using CRRES observations set we have shown that the maximum amplitude of the
476 annual variation in electron density is at American longitudes (about -60°E). This is in

477 good agreement with the analysis of Clilverd et al. [1991], and it seems very likely
478 that this is primarily caused by the influence of the Earth's tilted-offset dipole
479 magnetic field on the diffusive equilibrium conditions along the plasmaspheric field
480 lines, as represented by Figure 1 of this paper. The annual variation has an amplitude
481 of 2.7 at L=2.5 at solar maximum for American longitudes, which agrees with the
482 corresponding densities derived from ground-based observations of whistler-mode
483 signals. At New Zealand longitudes the ratio from CRRES observations was 1.5 for
484 L=2.5, which is also very close to the value found from whistler-mode signals taken
485 during the same period.

486

487 Several of the plasmaspheric models predicted that at Asian longitudes (+100°E) the
488 June densities would exceed the December densities, by typically a ratio of 1.2
489 [Guiter et al., 1995; Richards et al., 2000]. This result is not observed in the CRRES
490 data, where the ratio is 1.0 at almost all of the L-shells at this longitude. Guiter et al.
491 [1995] predicted that the December to June density ratio would increase slightly with
492 increasing L-shell. This is not observed at any of the longitudes studied in detail.

493

494 The CRRES data shows that the June electron density levels at American longitudes
495 are lower than for any other longitude. Clilverd et al. [1991] suggested that in June
496 there would be very little longitudinal variation in electron density, and estimated
497 Asian June density levels of 1000 el.cm^{-3} . This estimate was based on conjugate
498 pairs of ionosonde data, since no suitable whistler-mode data was available for the
499 Asian sector. For the African/Asian longitudes Nurmijarvi (60.5°N, 24.6°E) and
500 Kerguelen (49.4°S, 70.2°E) were analysed – mainly because of the lack of choice of
501 ionosonde stations in the southern hemisphere at these longitudes. These stations

502 represent $L=3.0-3.5$ conditions rather than $L=2.5$, and Figure 2 shows that typical
503 Asian electron density levels at these L -shells of ~ 3.0 are ~ 1000 el.cm⁻³, thus
504 explaining how the Asian sector equatorial electron density estimates of Clilverd et al.
505 [1991] were too low. The longitudinal variation of N_{eq} in June, although not
506 previously predicted, is consistent with a tilted offset dipole magnetic field effect on
507 plasmaspheric diffusive equilibrium conditions.

508

509 In Figure 4 we plotted the CRRES N_{eq} results in comparison with the model of
510 Carpenter and Anderson [1992] based on ISEE satellite data. The Carpenter and
511 Anderson (C&A) model results for December at solar maximum agree reasonably
512 well with the $L=2.5-4.0$ CRRES N_{eq} at American longitudes ($-60^\circ E$). At higher L -
513 shells the CRRES satellite observes lower density levels than the C&A model; this
514 may possibly be due to the CRRES data including unsaturated plasmasphere
515 conditions. In June at American longitudes ($-60^\circ E$) the C&A model over estimates the
516 electron density level consistently at all L -shells, and in December L -shells greater
517 than $L=3.5$ have consistently lower CRRES density levels than C&A. This appears to
518 be in part because of the influence of some unsaturated plasmasphere N_{eq} values in
519 the CRRES data, and also because of the lack of a longitudinal component in the
520 annual density variation of C&A.

521

522 Using the PADIE code and holding all variables constant apart from the background
523 electron density we find that hiss driven precipitation into the atmosphere will become
524 spectrally harder at American longitudes as the season changes from December to
525 June. At Asian longitudes there would be little change in the precipitation particle
526 energy spectra with season. An additional influence of the changing background

527 density in the plasmasphere could be on the generation and amplification of the hiss
528 waves themselves. If the source of free energy to drive the waves remains the same,
529 then reducing (increasing) the electron density should increase (decrease) the band of
530 frequencies generated, affecting the resonant energies. So, although here we have
531 shown that the annual changes in background electron density have an influence on
532 the dynamics of radiation belt particles, the picture is far from complete and requires
533 further study. Additionally, experimental evidence of this effect on the radiation belt
534 particles has yet to be published.

535

536 Summary

537

538 We have used CRRES measurements of plasmaspheric equatorial electron density
539 at solar maximum to investigate the longitudinal and annual variation in density in the
540 range $L=2.5-5.0$. We find that the largest annual variation occurs at American
541 longitudes (-60°E), and that no annual variation occurs at Asian longitudes ($+100^\circ\text{E}$).
542 These findings are in agreement with Clilverd et al. [1991]. The underlying cause is
543 due to the influence of a tilted-offset dipole geomagnetic field. At American
544 longitudes there is the largest discrepancy between geomagnetic latitude and
545 geographic latitude. This leads to substantial annual variations in ionospheric plasma
546 density, which map up into the plasmasphere as a consequence of diffusive
547 equilibrium.

548

549 Plasmaspheric electron density is larger in December than in June in the region
550 covering -180°E to $+20^\circ\text{E}$. Elsewhere the ratio of December to June is very close to
551 1.0. The annual variation also differs with L-shell. At American longitudes (-60°E),

552 and possibly at New Zealand longitudes, the maximum December/June ratio is at
553 $L=2.5-3.5$, with a value of 2.7 at American longitudes at solar maximum. At $L=4.5$
554 and above the annual variation disappears, possibly because the plasmasphere is not in
555 diffusive equilibrium with the ionosphere at these high L-shells, or the inclusion of
556 non-saturated electron density values from CRRES observations. The lowest electron
557 density values for a given L-shell occur at American longitudes. This is particularly
558 clear for the lower L-shells, although apparent as far out as $L=4.5$. These values occur
559 in June. Clearly the plasmasphere is strongly controlled by the configuration of the
560 Earth's magnetic field and the annual variations in the F2 regions that are in diffusive
561 equilibrium with it.

562

563 Ion densities also show significant annual variations. There are similar longitudinal
564 characteristics in the case of IMAGE EUV He^+ measurements taken during June and
565 December 2001. However, there are as yet unexplained differences in atomic mass
566 density measurements calculated using the magnetometer cross-phase technique,
567 where European values are significantly higher than those at American longitudes and
568 require a large correction factor for the ion composition.

569

570 Calculations of the effect of changing plasmaspheric density on wave-particle
571 interactions with plasmaspheric hiss indicate that the depletion of the plasmasphere at
572 American longitudes in June results in a harder energy spectrum of electrons being
573 precipitated into the atmosphere at those longitudes than anywhere else. Conversely,
574 the softest energy spectrum occurs at the same longitudes in December. Little
575 variation in precipitation energy spectrum is likely at Asian longitudes due to the
576 absence of any significant annual variation in plasmaspheric density.

577

577

578 References

579

580 Anderson, R. R., D. A. Gurnett, D. I. Odem (1992), CRRES Plasma-Wave
581 Experiment, *Journal Of Spacecraft And Rockets*, 29 (4), 570-573.

582

583 Berube, D., M. B. Moldwin, and J. M. Weygand (2003), An automated method for the
584 detection of field line resonance frequencies using ground magnetometer techniques,
585 *J. Geophys. Res.*, 108, 1348, doi:10.1029/2002JA009737.

586

587 Carpenter, D.L., and R.R. Anderson (1992), An ISEE/whistler model of equatorial
588 electron-density in the magnetosphere, *J. Geophys. Res.*, 97, 1097-1108.

589

590 Chappell, C. R., K. K. Harris, G. W. Sharp (1970), Morphology of bulge region of
591 plasmasphere, *J. Geophys. Res.*, 75 (19), 3848-3861.

592

593 Clilverd, M. A., A. J. Smith, and N. R. Thomson (1991), The annual variation in quiet
594 time plasmaspheric electron density determined from whistler mode group delays,
595 *Planet. Space Sci.*, 39, 1059-1067.

596

597 Clilverd, M. A., N. R. Thomson, and A. J. Smith (1992), Observation of two preferred
598 propagation paths for VLF signals received at a non-conjugate location, *J. Atmos.*
599 *Terr. Phys.*, 54, 1075-1079.

600

601 Clilverd, M. A., F. W. Menk, G. Milinevski, B. R. Sandel, J. Goldstein, B. W.
602 Reinisch, C. R. Wilford, M. C. Rose, N. R. Thomson, K. H. Yearby, G. J. Bailey, I. R.
603 Mann, and D. L. Carpenter (2003), In-situ and ground-based intercalibration
604 measurements of plasma density at L=2.5, *J. Geophys. Res.*, 108,
605 doi:10.1029/2003JA009866.
606
607 Gallagher, D. L., M. L. Adrian, and M. W. Liemohn (2005), Origin and evolution of
608 deep plasmaspheric notches, *J. Geophys. Res.*, 110, A09201,
609 doi:10.1029/2004JA010906.
610
611 Glauert, S. A., and R. B. Horne (2005), Calculation of pitch angle and energy
612 diffusion coefficients with the PADIE code, *J. Geophys. Res.*, 110, A04206,
613 doi:10.1029/2004JA010851.
614
615 Guiter, S. M., C. E. Rasmussen, T. I. Gombosi, J. J. Sojka, and R. W. Shunk (1995),
616 What is the source of observed annual variations in plasmaspheric density, *J.*
617 *Geophys. Res.*, 100, 8013-8020.
618
619 Gurnett, D. A., and R. R. Shaw (1973), Electromagnetic radiation trapped in the
620 magnetosphere above the plasma frequency, *J. Geophys. Res.*, 78, 8136-8149.
621
622 Helliwell, R. A. (1965), *Whistlers and related ionospheric phenomena*, Stanford
623 University Press, Stanford, California.
624

625 Horne, R. B., S. A. Glauert, and R. M. Thorne (2003), Resonant diffusion of radiation
626 belt electrons by whistler-mode chorus, *Geophys. Res. Lett.*, 30(9), 1493,
627 doi:10.1029/2003GL016963.

628

629 Lyons, L. R., R. M. Thorne, and C. F. Kennel (1972), Pitch angle diffusion of
630 radiation belt electrons within plasmasphere, *J. Geophys. Res.*, 77, 3455-3474.

631

632 Menk, F. W., D. Orr, M. A. Clilverd, A. J. Smith, C. L. Waters, and B. J. Fraser
633 (1999), Monitoring spatial and temporal variations in the dayside plasmasphere using
634 geomagnetic field line resonances, *J. Geophys. Res.*, 104, 19955-19970.

635

636 Menk, F. W., C. L. Waters, and B. J. Fraser (2000), Field line resonances and
637 waveguide modes at low latitudes, 1. Observations, *J. Geophys. Res.*, 105, 7747-7761.

638

639 Meredith, N.P., R. B. Horne, R. M. Thorne, D. Summers, and R.R. Anderson (2004),
640 Substorm dependence of plasmaspheric hiss, *J. Geophys. Res.*, 109, A06209,
641 doi:1029/2004JA010387.

642

643 Meredith, N.P., R. B. Horne, S. A. Glauert, R. M. Thorne, D. Summers, J. M.
644 Albert, and R.R. Anderson (2006), Energetic outer zone electron loss timescales
645 during low geomagnetic activity, *J. Geophys. Res.*, 111, A05212,
646 doi:10.1029/2005JA011516.

647

648 Olson, W. P., and K. Pfizter (1977), Magnetospheric magnetic field modelling,
649 Annual Scientific Report, AFOSR Contract No. F44620-75-c-0033.
650

651 Orr, D., and J. A. D. Matthew (1971), The variation of geomagnetic micropulsation
652 periods with latitude and the plasmapause, *Planet. Space Sci.*, 19, 897-904.
653

654 Park, C. G., D. L. Carpenter, and D. B. Wiggin, (1978), Electron density in the
655 plasmasphere: whistler data on solar cycle, annual and diurnal variations, *J. Geophys.*
656 *Res.*, 83, 3137-3144.
657

658 Rasmussen, C. E., and R. W. Shunk (1990), A three-dimensional time-dependent
659 model of the plasmasphere, *J. Geophys. Res.*, 95, 6133-6144.
660

661 Richards, P. G., T. Chang, and R. H. Comfort (2000), On the causes of the annual
662 variation in the plasmaspheric electron density, *J. Geophys. Res.*, 62, 935-946.
663

664 Rippeth, Y., R. J. Moffett, and G. J. Bailey (1991), Model plasmasphere calculations
665 for L-values near 2.5 at the longitude of Argentine Islands, Antarctica, *J. Atmos. Terr*
666 *Phys.*, 53, 551-555.
667

668 Rozanov, E., L. Callis, M. Schlesinger, F. Yang, N. Andronova, and V. Zubov (2005),
669 Atmospheric response to NO_y source due to energetic electron precipitation, *Geophys.*
670 *Res. Lett.*, 32, L14811, doi:10.1029/2005GL023041.
671

672 Sandel B.R., R.A. King, W.T. Forrester, D.L. Gallagher, A. L. Broadfoot, C.C. Curtis
673 (2001), Initial results from the IMAGE extreme ultraviolet imager, *Geophys. Res.*
674 *Lett.*, 28, 1439-1442.
675

676 Sandel, B. R., J. Goldstein, D. L. Gallagher, and M. Spasojević (2003), Extreme
677 ultraviolet imager observations of the structure and dynamics of the plasmasphere,
678 *Space Sci. Rev.*, 109, 25-46.
679

680 Saxton, J. M., and A. J. Smith (1989), Quiet time plasmaspheric electric fields and
681 plasmasphere-ionosphere coupling fluxes at $L = 2.5$, *Planet. Space Sci.*, 37, 283-293.
682

683 Singer, H. J., W. P. Sullivan, P. Anderson, F. Mozer, P. Harvey, J. Wygant, and W.
684 McNeil (1992), Fluxgate magnetometer instrument on the CRRES, *J. Spacecr.*
685 *Rockets*, 29, 599-601.
686

687 Strangeways, H. J. (1991), The upper cutoff frequency of nose whistlers and
688 implications for duct structure, *J. Atmos. Terr. Physics*, 53, 151-169.
689

690 Sutcliffe, P. R., S. K. F. Hattingh, and H. F. V. Boshoff (1987), Longitudinal effects
691 on the eigenfrequencies of low-latitude Pc3 pulsations, *J. Geophys. Res.*, 92, 2535-
692 2543.
693

694 Tarcsai, G., P. Szemeredy, and L. Hegymegi (1988), Average electron density profiles
695 in the plasmasphere between $L=1.4-3.2$ deduced from whistlers, *J. Atmos. Terr.*
696 *Phys.*, 50, 607-611.

697

698 Taylor, J. P. H., and A. D. M. Walker (1984), Accurate approximate formulae for
699 toroidal standing hydromagnetic oscillations in a dipolar geomagnetic field, *Planet.*
700 *Space Sci.*, 32, 1119-1124.

701

702 Walker, A. D. M., J. M. Ruohoniemi, K. B. Baker, R. A. Greenwald, and J. C.
703 Samson (1992), Spatial and temporal behaviour of ULF pulsations observed by the
704 Goose Bay HF radar, *J. Geophys. Res.*, 97, 12187-12202.

705

706 Waters, C. L., F. W. Menk, and B. J. Faser (1994), Low latitude geomagnetic field
707 line resonance; experiment and modelling, *J. Geophys. Res.*, 99, 17547-17558.

708

709 Webb, P. A., and E. A. Essex (2001), A dynamic diffusive equilibrium model of the
710 ion densities along plasmaspheric magnetic flux tubes, *J. Atmos. Solar Terr. Phys.*,
711 63, 1249-1260.

712

713 CLILVERD ET AL.: PLASMASPHERIC DENSITY VARIATIONS

714 Figure 1. The variation of the geographic latitudes of the footprints of the L=2.5 field
715 line, showing significant changes in relative latitude in the longitude region of -60°E.
716

717 Figure 2. The longitudinal variation of equatorial electron density from the CRRES
718 data plotted for a range of L-shells. Data from the December solstice (solid lines) are
719 compared with data from the June solstice (dashed line). An error bar is shown
720 representing one standard deviation in the data.
721

722 Figure 3. The variation of the December/June ratio with L-shell, at the longitudes of
723 Asia, America, and New Zealand/Pacific, derived from the CRRES data.
724

725 Figure 4. The radial profile of equatorial electron densities from CRRES data for a
726 range of L-shells and longitudes (diamonds). Standard deviations for the data are
727 shown. A fit to the data is given by the solid line, expressed in terms of P_e and N from
728 equation (1). The Carpenter and Anderson (1992) model results for solar maximum
729 conditions and low magnetic activity are also shown (dotted lines).
730

731 Figure 5. The CRRES equatorial electron density variation with longitude at L=2.5 for
732 December (solid line) and June (dashed line). The longitudinal variation of IMAGE
733 EUV He^+ abundances in 2001 for December (crosses) and June (diamonds) are shown
734 in comparison, using the right-hand y-scale). Ion number densities from ground-based
735 cross-phase techniques are shown for December (squares) 2003 and June 2001
736 (triangles) using the atomic mass unit adjusted by a weighting factor – see text for
737 more details.
738

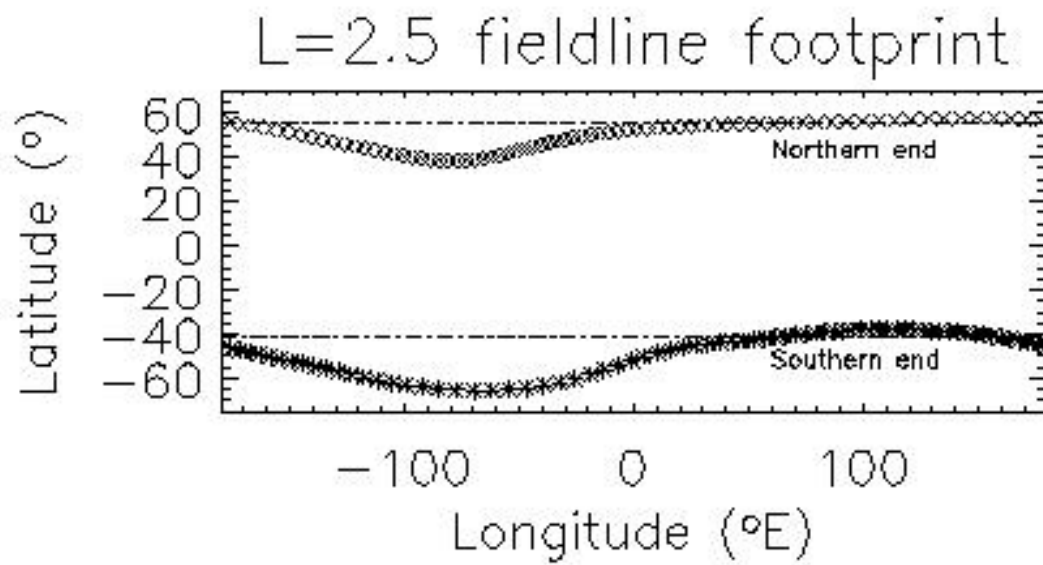
739

740 Figure 6. PADIE results for pitch angle diffusion coefficients at 100 keV, 300keV,
741 and 1 MeV due to plasmaspheric hiss, for a range of plasmaspheric density conditions
742 equivalent to density levels of 1500 el.cm^{-3} ($f_{pe}/f_{ce}=10.8$), 1000 el.cm^{-3} ($f_{pe}/f_{ce}=8.8$),
743 and 500 el.cm^{-3} ($f_{pe}/f_{ce}=6.2$) at $L=3.0$. The edge of the loss cone is indicated by a
744 vertical dot-dashed line.

745

746

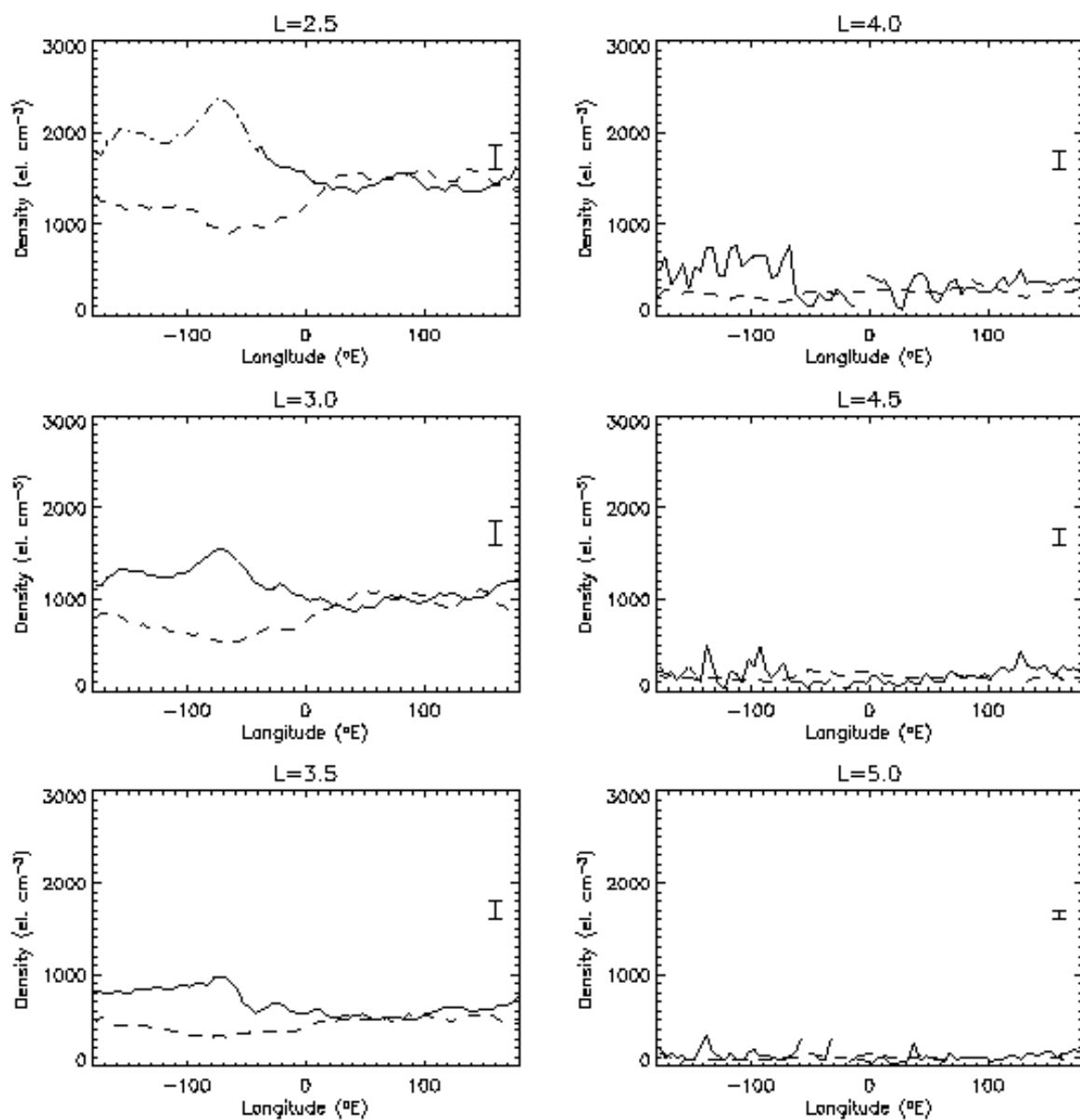
747



747

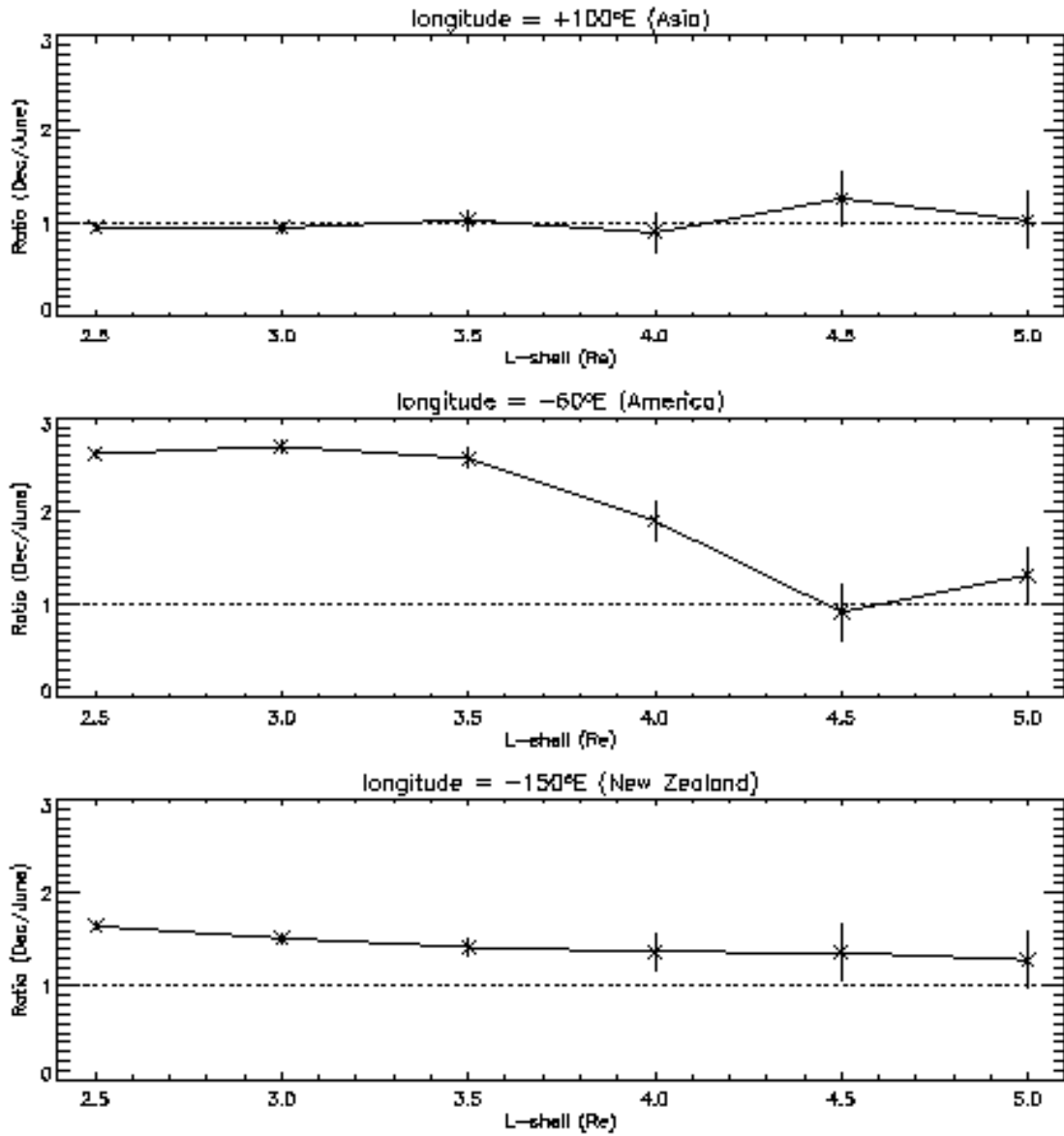
748 Figure 1. The variation of the geographic latitudes of the footprints of the L=2.5 field
749 line, showing significant changes in relative latitude in the longitude region of -60°E.
750

750
751
752



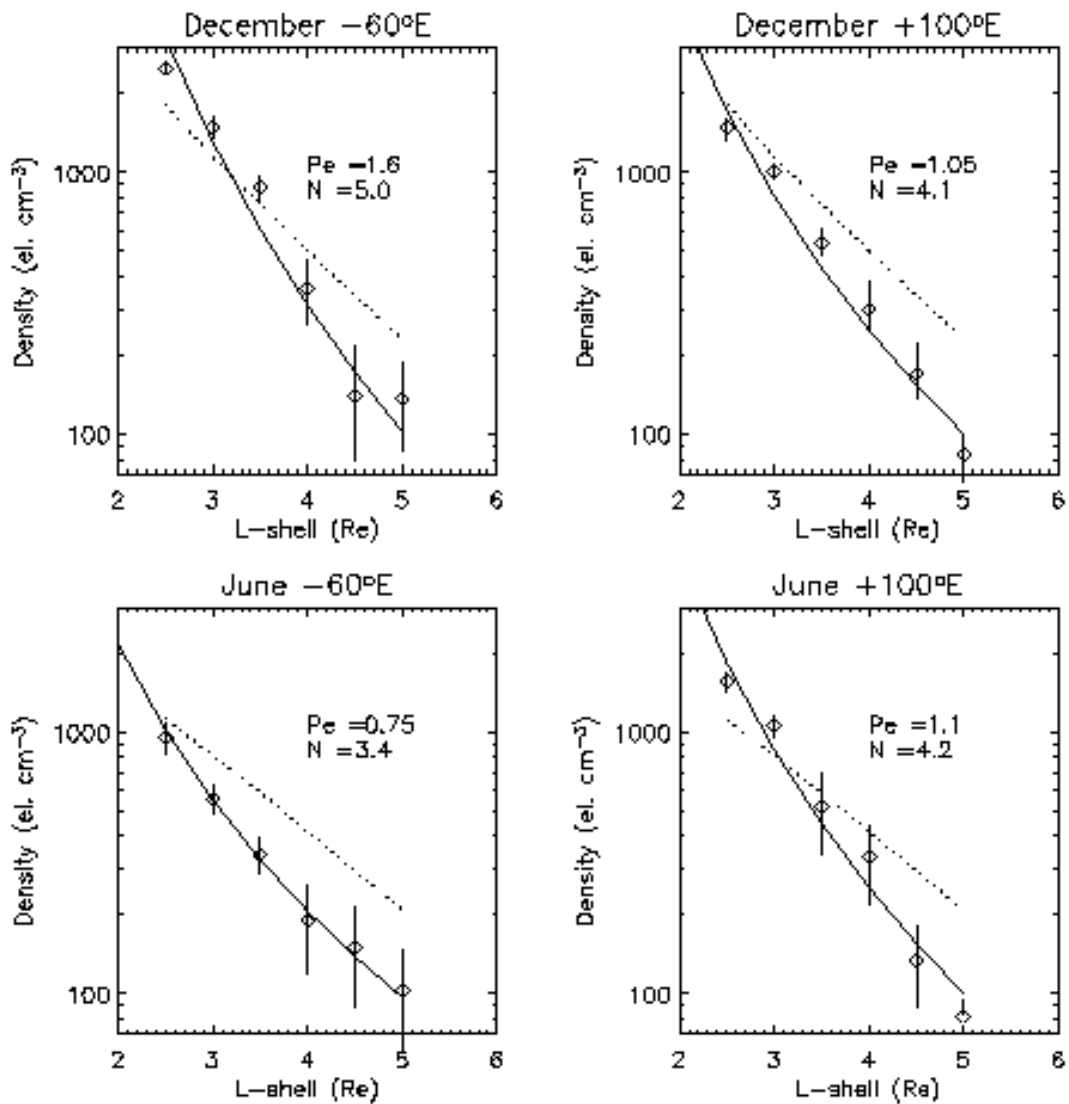
753
754
755
756
757
758
759

Figure 2. The longitudinal variation of equatorial electron density from the CRRES data plotted for a range of L-shells. Data from the December solstice (solid lines) are compared with data from the June solstice (dashed line). An error bar is shown representing one standard deviation in the data.



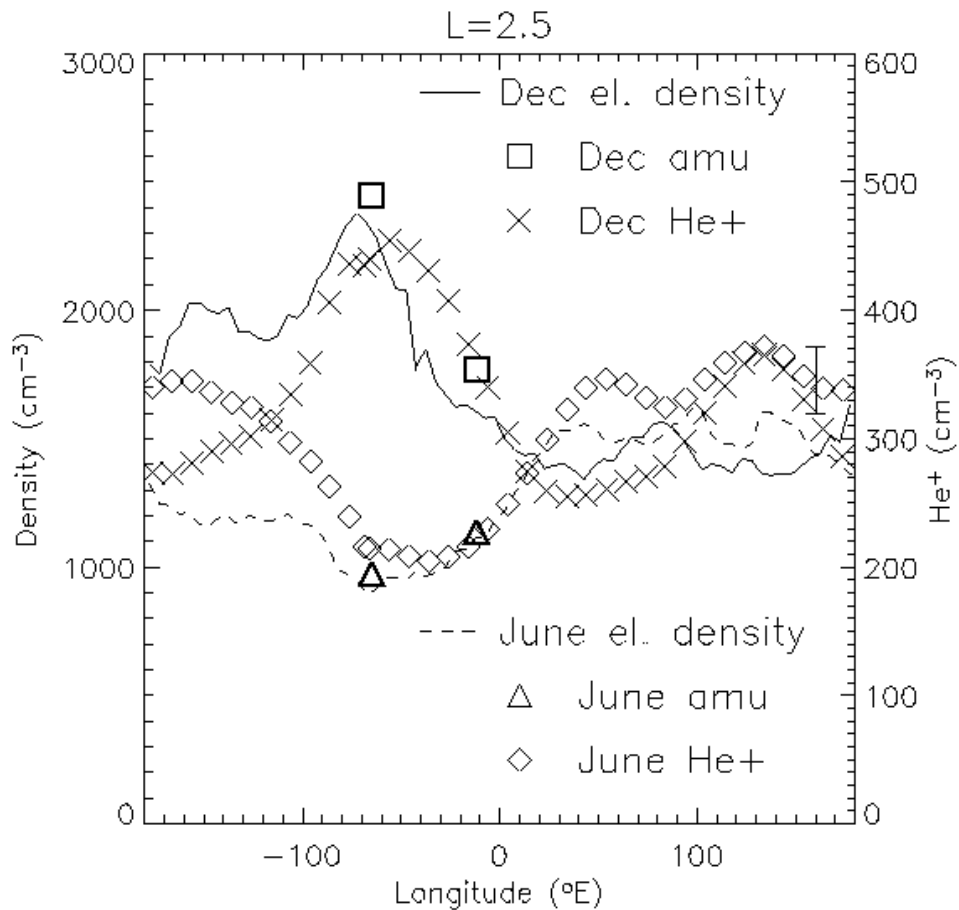
760
 761
 762
 763
 764
 765

Figure 3. The variation of the December/June ratio with L-shell, at the longitudes of Asia, America, and New Zealand/Pacific, derived from the CRRES data.



766
 767
 768
 769
 770
 771
 772
 773
 774

Figure 4. The radial profile of equatorial electron densities from CRRES data for a range of L-shells and longitudes (diamonds). Standard deviations for the data are shown. A fit to the data is given by the solid line, expressed in terms of Pe and N from equation (1). The Carpenter and Anderson (1992) model results for solar maximum conditions and low magnetic activity are also shown (dotted lines).

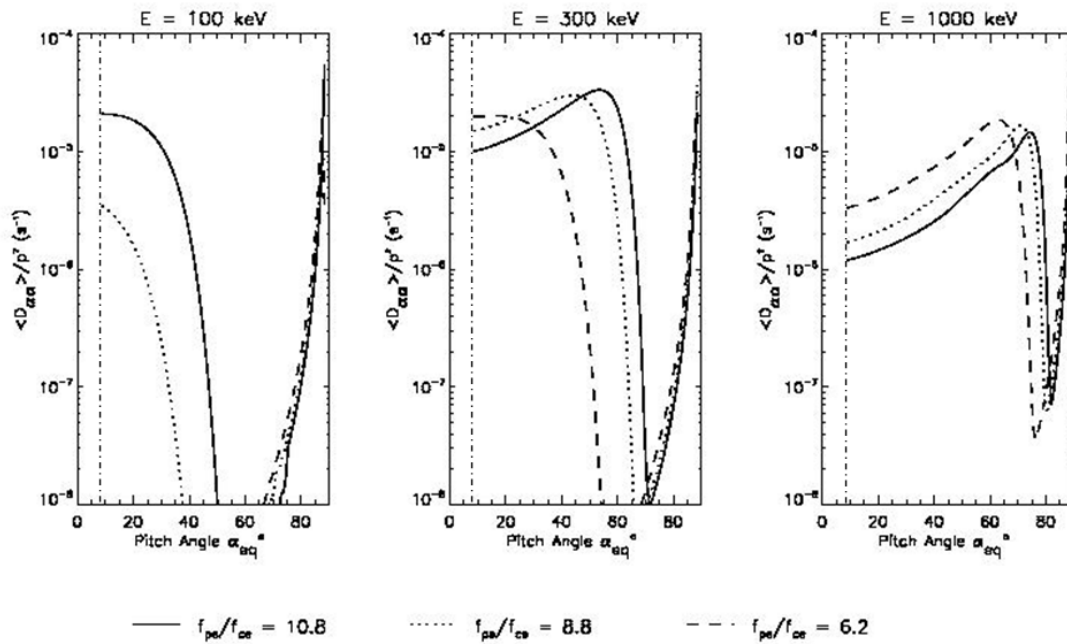


775

776

777 Figure 5. The CRRES equatorial electron density variation with longitude at L=2.5 for
 778 December (solid line) and June (dashed line). The longitudinal variation of IMAGE
 779 EUV He⁺ abundances in 2001 for December (crosses) and June (diamonds) are shown
 780 in comparison, using the right-hand y-scale). Ion number densities from ground-based
 781 cross-phase techniques are shown for December (squares) 2003 and June 2001
 782 (triangles) using the atomic mass unit adjusted by a weighting factor – see text for
 783 more details.

784



785
 786 Figure 6. PADIE results for electron pitch angle diffusion coefficients at 100 keV,
 787 300keV, and 1 MeV due to plasmaspheric hiss, for a range of plasmaspheric density
 788 conditions equivalent to density levels of 1500 el.cm^{-3} ($f_{\text{pe}}/f_{\text{ce}}=10.8$), 1000 el.cm^{-3}
 789 ($f_{\text{pe}}/f_{\text{ce}}=8.8$), and 500 el.cm^{-3} ($f_{\text{pe}}/f_{\text{ce}}=6.2$) at $L=3.0$. The edge of the loss cone is
 790 indicated by a vertical dot-dashed line.

791
 792
 793
 794
 795
 796
 797
 798
 799
 800
 801
 802
 803
 804
 805
 806
 807